Available online at www.sciencedirect.com
SCIENCE DIRECT®
International Journal of Heat and Mass Transfer 49 (2006) 1928–1936
International Journal of HEAT and MASS TRANSFER
www.elsevier.com/locate/ijhmt

Effect of the dielectric transition on laser-induced phase explosion in metals

Cristian Porneala, David A. Willis *

Department of Mechanical Engineering, Southern Methodist University, P.O. Box 701923, Dallas, TX 75275, USA

Received 24 May 2005; received in revised form 8 November 2005
Available online 6 January 2006

Abstract

Phase explosion is an explosive liquid to vapor phase change that occurs during laser ablation as the surface approaches 90% of the thermodynamic critical temperature ($0.9T_c$), which is the upper limit of superheating. Large variations in properties are expected to occur near $0.8T_c$, transforming the electrically conductive metal into a nearly transparent dielectric, an effect that has been neglected in previous models of laser ablation. The work presented in this paper numerically investigates the possible effect of the dielectric transition using a one dimensional heat transfer model. The results show that accurate knowledge of the absorption coefficient above $0.8T_c$ is critical for predicting the laser fluence at which phase explosion occurs.

Keywords: Dielectric transition; Phase explosion; Laser ablation; Micromachining

1. Introduction

Phase explosion is an explosive liquid–vapor phase change that occurs as a result of homogeneous nucleation of vapor in a superheated liquid [1]. A p–T diagram of a typical metal in the neighborhood of the critical point provides a clear insight into the mechanism of phase explosion and homogeneous nucleation. Fig. 1 is a representative p–T diagram obtained from low T_c metals such as cesium and mercury [2]. The binode line in Fig. 1 corresponds to the liquid metal in equilibrium with saturated metal vapor. During heating by laser pulses with durations less than about 1 μs (10^{-6} s) liquid superheating above the binode may occur since heterogeneous nuclei (initiated from a variety of disturbances or defects) will not have significant time to grow, preventing normal boiling [3,4]. If the laser pulse energy is high enough, the surface temperature deviates from the binode into the metastable region, and approaches the spinode, which is the boundary of thermodynamic stability. As the temperature approaches the spinode ($\sim 0.9T_c$ at p_{atm}), the rate of homogeneous nucleation rises rapidly, resulting in phase explosion. Prior to reaching the spinode, the superheated liquid experiences large density fluctuations at $0.8T_c$, referred to as the "onset of anomalies." Associated with the onset of anomalies is an increase of electrical resistance due to electron scattering by density fluctuations and localization of electrons. Thus at the onset of anomalies, the metallic conductivity and the associated reflectivity and absorption coefficient decrease jump-wise and the liquid metal becomes a liquid dielectric. As a result, the material becomes almost transparent and weakly absorbing to the incident radiation. This process is commonly referred to as the "dielectric transition."

Previous numerical studies of phase explosion showed monotonic heating of the surface up to $0.9T_c$ and neglected the dielectric transition when calculating the threshold fluence required to reach $0.9T_c$ [5–7]. Song and Xu [8], showed that for metals, phase explosion occurs during laser pulse. Although the concept of a dielectric, or transparency wave was predicted by Batanov et al. [9], its effect on laser ablation has not been studied in detail. Yoo et al. [10], assuming that the liquid metal transforms into a dielectric and becomes

* Corresponding author. Tel.: +1 214 768 3125; fax: +1 214 768 1473.
E-mail address: dwillis@engr.smu.edu (D.A. Willis).

0017-9310/$ - see front matter © 2005 Elsevier Ltd. All rights reserved.
doi:10.1016/j.ijheatmasstransfer.2005.11.005

Nomenclature

a	absorption coefficient (m^{-1})
B	sticking coefficient
c_p	specific heat (J/kg K)
c	speed of light in vacuum (m/s)
d	thickness of the dielectric layer (m)
f	liquid fraction
H	enthalpy (J/kg)
I_a	absorbed laser fluence (J/m^2)
I_{max}	maximum laser fluence (J/m^2)
I_0	incident laser fluence (J/m^2)
k	thermal conductivity (W/m K)
k_B	Boltzman constant (J/K)
k_0	propagation constant (m^{-1})
L	latent heat (J/kg)
$\dot{M}$	mass flux leaving the surface (kg/m^2 s)
m_a	atomic mass of a molecule (kg/molecule)
p	pressure (N/m^2)
$\dot{q}$	volumetric heat generation (W/m^3)
R	reflectivity of the target surface
R_{gas}	gas constant of vapor (J/kg K)
T	temperature (K)
t	time (s)
t_{max}	time when laser energy is at its maximum (s)
x	coordinate normal to the target surface (m)

Greek symbols

ε_0	permittivity of vacuum ($C^2/N\ m^2$)
λ	laser light wavelength (nm)
θ	parameter characterizing the laser pulse temporal profile
ρ	density (kg/m^3)
σ	electrical conductivity ($\Omega^{-1}\ m^{-1}$)
τ	pulse width (s)
ϵ	dielectric constant

Subscripts

atm	ambient atmospheric conditions
b	equilibrium boiling point
c	critical point
d	dielectric layer
l	liquid
lv	liquid–vapor phase change
m	melting point
new	value at the current time step
old	value at the previous time step
s	solid
sat	saturation value
sl	solid–liquid phase change

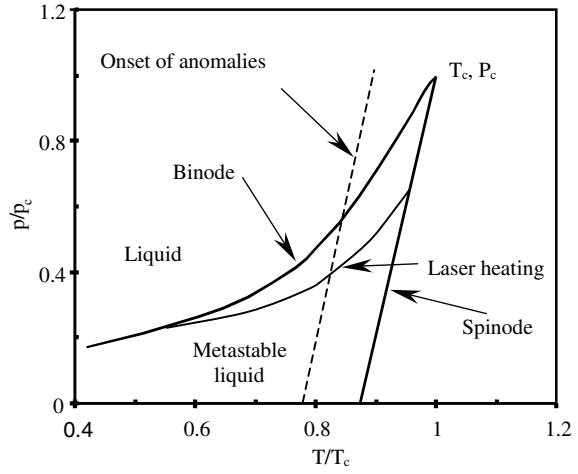

Fig. 1. Pressure–temperature diagram for a typical metal [2].

optically transparent at $0.9T_c$, computed the thickness of the dielectric layer. The computed thickness of the dielectric layer long after the laser pulse shows that the superheated state is maintained long enough to ensure the growth of the homogeneous nuclei to a critical size, an essential condition for phase explosion to take place. Thus, phase explosion occurred long after the end of the laser pulse.

The present work numerically investigates the theoretical impact of the dielectric transition upon short pulse laser ablation of metals. In this paper we describe a model developed to solve the heat transfer in the target accounting for conduction, melting, and the dielectric transition. The computations predict the transient temperature field, melt depth, and thickness of the dielectric layer. An estimate of the absorption coefficient of the dielectric liquid was calculated using the available literature, and was included in the model.

2. Numerical model

Numerical modeling was performed using the finite difference method to compute the heat transfer and phase change processes during the laser interaction with aluminum. The calculation accounts for the reflection and absorption of the laser beam, heat diffusion, and melting in the material. The variation of optical properties of the material due to the dielectric transition is considered in order to predict the transient depth of the dielectric layer and the change in laser fluence required to reach $0.9T_c$.

2.1. Governing equations

A one-dimensional numerical model is developed to compute the heat flow and phase change during high power laser ablation of aluminum. A one-dimensional assumption is valid as long as the laser spot size is much larger than the thermal diffusion length, which is of the order of a few micrometers for nanosecond laser irradiation of metals.

During laser interaction with metals, energy is transferred to the lattice through electron phonon collisions, and induces target heating. The electron phonon thermalization time for aluminum was estimated to be 130 fs, considering the available data [11–13]. Since the heating time (nanosecond and picosecond heating regimes) considered in this work is much greater than the estimated value of the thermalization time, the energy transfer induced by laser irradiation in the solid and liquid aluminum is governed by the heat diffusion equation, which is based on Fourier's law of conduction:

$$\rho c_p \frac{\partial T}{\partial t} = \nabla(k\nabla T) + \dot{q} \tag{1}$$

where T, c_p, ρ, and k are, respectively, temperature, specific heat, density, and thermal conductivity. The volumetric heating term in Eq. (1) is used to describe the nonuniform absorption of the laser energy in the target and will be described further in Section 3.

It was estimated that during the laser pulse, thermal emission of radiation from the surface and convection are at least two orders of magnitude smaller than the incident laser irradiance and the conduction heat transfer. Since the focus of this study is to highlight the importance of the change in optical properties during the metal-dielectric transition, neglecting thermal emission and convection would not significantly affect the temperature history and the results of this work. It was also assumed that the ablation plume that may be present during the laser pulse due to evaporation process does not hinder the laser energy incident to the target.

Considering the previous assumptions, the following initial and boundary conditions may be assumed:

$$T(x,t)|_{t=0} = T_{\text{atm}} \tag{2}$$

$$T(x,t)|_{x\to\infty} = T_{\text{atm}} \tag{3}$$

where T_{atm} is the surrounding temperature ($T_{\text{atm}} = 300$ K).

When the vaporization exists at the surface the energy loss due to evaporation can be calculated as the product of the latent heat of vaporization and the mass flux leaving the surface. In order to obtain an order of magnitude estimate of the heat loss at the liquid surface, the mass loss was calculated based on the Hertz–Knudsen equation (Eq. (4)) for a surface temperature of $0.8T_c$ for a period of 10 ns.

$$\dot{M} = m_a \frac{0.82 B p_{\text{sat}}}{(2\pi m_a k_B T)^{0.5}} \tag{4}$$

where the sticking coefficient, B, was set to a value of 1 [14]. The coefficient of 0.82 accounted for the backflow of vapor to the surface due to collisions with other vaporized atoms [15]. The saturation pressure (p_{sat}) is obtained from the Clausius–Clapeyron equation:

$$p_{\text{sat}} = p_{\text{atm}} \exp\left[\frac{L_{\text{lv}}(T - T_b)}{R_{\text{gas}} T T_b}\right] \tag{5}$$

According to the calculations, the heat loss due to evaporation was estimated to be three orders of magnitude smaller than the laser fluence on the surface. The fluence to reach $0.9T_c$ will not be altered significantly by this heat loss, thus the boundary condition on the free surface is described by a zero heat flux condition:

$$-k\left.\frac{\partial T}{\partial x}\right|_{x=0,t} = 0 \tag{6}$$

2.2. Phase change model

In the present work, the enthalpy technique is used to handle the phase change that includes a liquid–solid interface. The use of this method assumes that the phase change occurs over a small temperature range between T_s and T_l. The melt interface is not tracked explicitly using a system of coordinates attached to the moving interface. Instead, the liquid fraction, which indicates the fraction of the cell volume that is in liquid form, is computed at each iteration based on an enthalpy balance. The energy equation is reformulated in terms of enthalpy per unit volume as:

$$\frac{\partial H}{\partial t} = \nabla(k\nabla T) + \dot{q} \tag{7}$$

In Eq. (7), the averaged enthalpy value H within a control volume can be written in terms of sensible enthalpy and latent heat content (fL_{sl}) as follows:

$$H = \int_{T_{\text{atm}}}^{T} \rho c \, \mathrm{d}T + fL_{\text{sl}} \tag{8}$$

The latent heat content ($\Delta H = fL_{\text{sl}}$) in Eq. (8), depends on the temperature and may vary between zero (solid) and L_{sl} (liquid), the latent heat of melting. Thus, the liquid fraction, f, can vary between zero and one depending on the temperature, as follows:

$$\begin{aligned} f &= \frac{\Delta H}{L_{\text{sl}}} = 0 \quad T < T_s \\ f &= \frac{\Delta H}{L_{\text{sl}}} = 1 \quad T > T_s \\ f &= \frac{\Delta H}{L_{\text{sl}}} = \frac{T - T_s}{T_l - T_s} \quad T_s < T < T_l \end{aligned} \tag{9}$$

Once the liquid fraction is calculated, the averaged enthalpy value H within a control volume is computed based on Eq. (8). The solution for temperature is essentially an iteration between enthalpy (provided by Eq. (8)), and the energy equation (Eq. (7)) that updates the values of the temperature.

3. Optical properties and the dielectric transition

Prior to reaching $0.8T_c$, the energy absorbed may be represented as a heat source within the material having a rate of heat generation per unit volume, ($\dot{q}$) given as:

$$\dot{q} = -\frac{\mathrm{d}I_a}{\mathrm{d}x} = a(1-R)I_0 \mathrm{e}^{-ax} \tag{10}$$

where a is the absorption coefficient and R is the surface reflectivity.

During the laser heating, the target surface is assumed to be irradiated by a single laser pulse having an incident temporal profile given by:

$$I_0 = I_{\max}\left(\frac{t}{t_{\max}}\right)^{\theta} \exp\left[\theta\left(1-\frac{t}{t_{\max}}\right)\right] \tag{11}$$

where $I_{\max}$ is the peak value of the laser irradiance, $t_{\max}$ represents the time when the laser energy is at its maximum and parameter $\theta = 7$ was chosen to fit a typical pulse provided by a Nd:YAG. The same value of $\theta = 7$ was chosen to characterize the temporal variation of the laser intensity during the picosecond laser heating. Therefore, the shape of the laser pulse remains identical for both heating regimes and the time scale is set only by choosing different values for $t_{\max}$.

Batanov et al. [9] predicted that when the laser intensity is high enough to heat the sample near the critical temperature (between 10^7 and 10^8 W/cm^2), a change in material properties occurs as a result of strong reduction of electron density. Therefore, the reflectivity and the absorption coefficients that depend on the electron density (hence on the temperature) decrease jump-wise and the liquid metal becomes a liquid dielectric. As a result, near the critical temperature a liquid might become semi-transparent and only weakly absorbing to the incident irradiation. The incident laser energy penetrates through the dielectric layer to the underlying material that is still in the metallic state. During the formation of the induced dielectric layer, a new interface in the liquid metal occurs (Fig. 2).

The dielectric transition was modeled by assuming that for temperatures above $0.8T_c$, the superheated aluminum liquid is semi-transparent to the laser irradiation. The volumetric heat generation term given by Eq. (10) must be modified to account for the change in properties. The heat generation in the dielectric layer is given by:

$$\dot{q}_d = a_d(1-R_d)I_0 e^{-a_d x} \tag{12}$$

where a_d and R_d represent the absorption coefficient and surface reflectivity for the dielectric liquid, respectively.

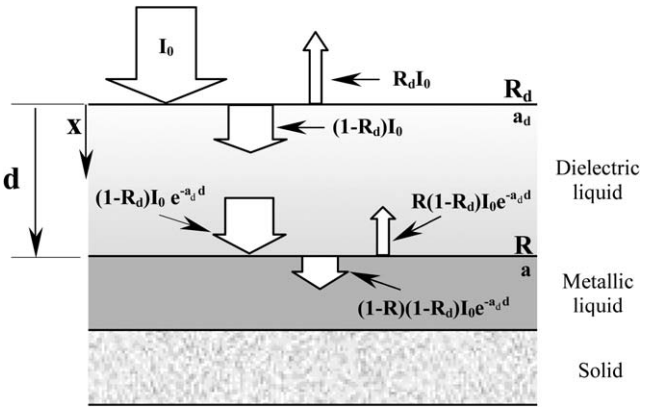

Fig. 2. Absorption of the laser light during dielectric transition.

During the formation of the dielectric layer the incident laser energy penetrates through the dielectric layer to the underlying material that is still in the metallic state. For the underlying metal the rate of heat generation is calculated by:

$$\dot{q}_l = a(1-R)(1-R_d)I_0 e^{-a_d d} e^{-a(x-d)} \tag{13}$$

where d is the transient thickness of the dielectric layer, and is calculated in the numerical code from the location at which the temperature has reached $0.8T_c$. In this study, the heat generation contribution resulting from absorption of the light reflected at the dielectric–metal liquid interface (RI_{0d}) was neglected. The drop in thermal conductivity associated with the dielectric transition was not included in the model. The drop in thermal conductivity is not expected to cause serious errors since the free surface has little heat loss. Thus, very little heat is expected to be conducted across the dielectric layer. Another assumption made in this study was to neglect interference effects between the incident beam and the beam reflected from the metal-dielectric interface.

In order to model the heat absorption by the dielectric layer an estimation of the absorption coefficient was made considering the available data. The value of the absorption coefficient evaluated at the room temperature ($a = 1.38\times10^8$ m^{-1}) was employed in our calculation to characterize the liquid metal below $0.8T_c$. The adopted value for the absorption coefficient has the same order of magnitude as the value estimated by Batanov et al. [9] to describe the energy deposition during the evaporation regime when the target surface remains a metal.

The following formula proposed by Batanov et al. was used in our calculation to account for the absorption coefficient in the dielectric layer:

$$a_d \approx \epsilon^{1/2} k_0 \frac{2\sigma\lambda}{\varepsilon_0 c} \tag{14}$$

where ϵ, k, σ, ε_0, c, $\lambda = 1064$ nm are the dielectric constant of the lattice, light propagation constant, electrical conductivity, permittivity of vacuum, speed of light and laser light wavelength, respectively. In our calculation, the value adopted for the dielectric constant (ϵ) of aluminum calculated at room temperature is 1 [16] and has the same order of magnitude as the dielectric constant of a typical condensed media proposed by Batanov to characterize the dielectric transition. It is known that when the density of a typical metal is near and below the critical density, the electrical conductivity falls by as much as eight orders of magnitude [17]. Using Eq. (14) and considering the decrease of electrical conductivity by eight orders of magnitude, the absorption coefficient of the dielectric layer was estimated to be $a_d = 1676$ m^{-1}($<0.01\%a$). In addition, due to a sudden decrease in electrical conductivity, the reflectivity of the aluminum in the vicinity of the dielectric transition drops to about 20% of the reflectivity value at room temperature [18]. During the heating time, the change in reflectivity of aluminum is not expected to be

as dramatic as the change experienced when the liquid reaches the dielectric transition. Therefore, the reflectivity value at room temperature ($R = 0.8$) was chosen to characterize the aluminum for temperatures below $0.8T_c$, while the reflectivity of the dielectric liquid surface is considered 0.2.

4. Computational method

Calculations were performed for two different pulse durations to characterize the laser heating of aluminum in nanosecond and picosecond regimes. Therefore, the value of t_{max} in Eq. (11) was set to values of 7 ns and 50 ps to describe the incident laser intensity temporal profile. The length of the computational domains (L) was chosen based on the thermal penetration depth during the heating processes and assuming that at $x = L$ the temperature of the material is unaffected by the laser irradiation. Therefore, using the estimates of the thermal penetration depth (2.1 μm and 0.2 μm for a pulse duration of 14 ns and 100 ps, respectively), L was set to a value of 7 μm and 2 μm to describe the energy deposition during nanosecond and picosecond laser heating, respectively. The discretization domain consists of fixed uniform grids in two regions. The region on the top of the sample exposed to the laser flux having a length comparable to the thermal penetration depth is discretized using 200 finite difference cells to accurately describe the absorption process inside the optical penetration depth. The second region was discretized using a coarse uniform grid consisting of 100 cells. Calculations were performed using variable time steps ranging between 1×10^{-14}–1×10^{-12} s and 1×10^{-16}–1×10^{-14} s for the nanosecond and picosecond regimes, respectively. The initial temperature of the material was 300 K. It was assumed that the melting is initiated at T_s and the mushy region is bounded by $T_s = T_m$ and $T_l = T_s + 0.1$ K. The thermal and optical properties of the aluminum used in the numerical model are given in Table 1. The quantities ρ, c_p, and k were assumed to be temperature independent.

Table 1
Thermal and optical properties used to describe laser ablation of Al [16,17,19]

Property	Value
Density, ρ (liquid, solid)	2700 (kg/m^3)
Melting temperature, T_m	933.5 (K)
Latent heat of fusion, L_{sl}	396,000 (J/kg)
Latent heat of vaporization, L_{lv}	105×10^5 (J/kg)
Specific heat, c_p (solid, liquid)	940 (J/kg K)
Thermal conductivity, k	235 (W/m K)
Critical temperature, T_c	5410 (K)
Boiling temperature at 1 atm, T_b	2793.15 (K)
Atomic mass, m_a	4.48×10^{-26} (kg/molecule)
Dielectric constant, ϵ at 293 K	1
Electrical conductivity, σ at 293 K	$3.54\times10^7\ \Omega^{-1}\ m^{-1}$

A segregated numerical method was used to solve the governing integral equation for energy. This approach solves for the unknown variable field by considering all cells at the same time. A first order implicit scheme was used to linearize the energy integral with respect to the temperature. The temperature in each cell is computed using a relation that includes both existing and unknown values from neighboring cells. Iteration for each time step were carried out until the temperature field converges according to the following criterion:

$$\left|\frac{H_{new} - H_{old}}{H_{old}}\right|_{grid=i} < 10^{-6} \tag{15}$$

5. Results

5.1. Nanosecond heating

The transient surface temperature during nanosecond laser heating is plotted in Fig. 3(a) for several values of laser fluence (J/cm^2). The results shown in this plot were obtained without considering the change in optical properties as the surface reached the dielectric transition at $0.8T_c$. The surface temperature reaches a maximum value soon after the peak of the laser pulse and then decreases gradually, as expected. Previous studies in the literature have considered phase explosion to occur when the surface temperature reached $0.9T_c$, which is approximately 4869 K for aluminum. Calculations were performed to find the laser fluence required to reach this temperature. The laser fluence required to reach $0.9T_c$ is 6.5 J/cm^2. At this temperature the phase explosion will occur, preventing further superheating of the liquid metal. Any further increase in fluence would only decrease the time at which the surface temperature reached the spinodal. In order to analyze the effect of the dielectric transition, the superheated liquid is assumed to be semi-transparent for temperatures above $0.8T_c$. When the change in optical properties was included in the model, a significant change in the surface temperature resulted. Several values of the absorption coefficient were chosen to model the absorption of heat within the dielectric layer. The first calculation was performed using an absorption coefficient of zero, and the results are shown in Fig. 3(b). Since there is no absorption of heat in the dielectric layer, the surface temperature never rises above $0.8T_c$. However, the transient thickness of the dielectric layer increased to a maximum value of 500 nm and decreased to a value of zero at the end of the laser pulse as shown in Fig. 4.

A second set of calculations computed the melting depth and the dielectric layer thickness using an absorption coefficient of $a_d = 1676\ m^{-1}$, as predicted by Eq. (14). Fig. 5 shows that unlike the dielectric layer thickness, which became zero at the end of the laser pulse, the melting depth grew monotonously during the laser pulse. It was also found that the melting depth does not depend on the absorption coefficient in the dielectric layer. In this case,

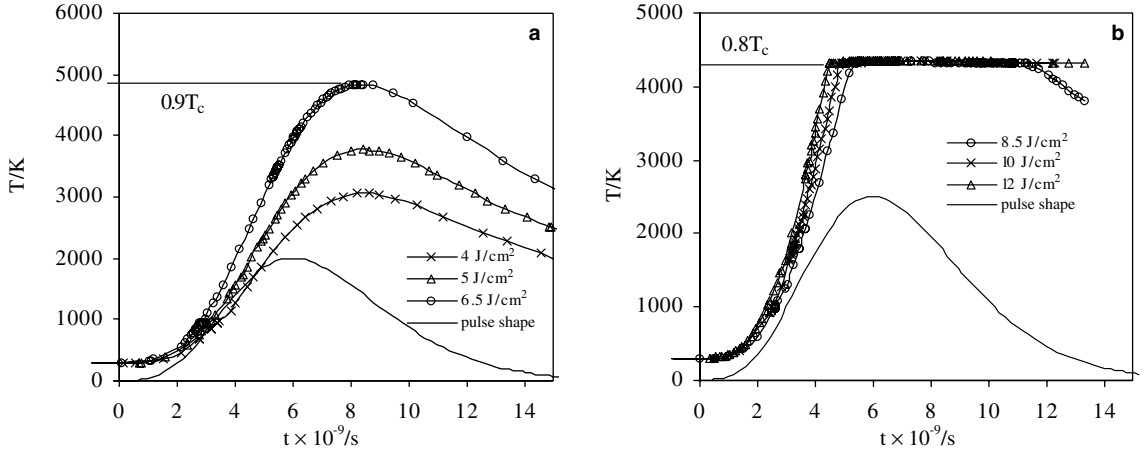

Fig. 3. Transient surface temperature for different laser fluences: (a) without considering dielectric transition; (b) considering dielectric transition at $0.8T_c$ ($\tau = 7$ ns (FWHM)).

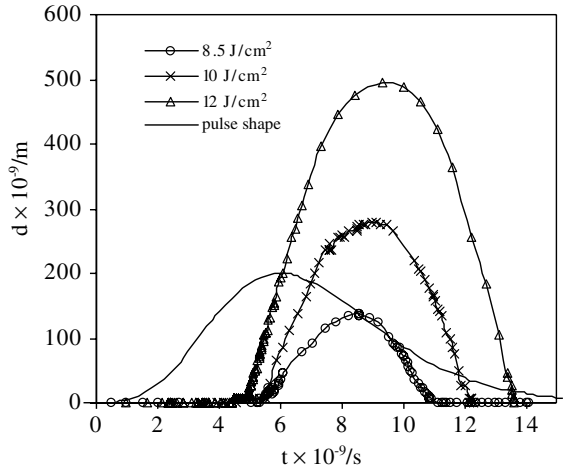

Fig. 4. Transient thickness of the dielectric layer for different laser fluences ($a_d = 0$, $\tau = 7$ ns (FWHM)).

the temperature profiles were not significantly altered from those seen in Fig. 3(b). This can be explained by the small value of the absorption coefficient (estimated by Eq. (14)) compared with the value that characterizes the material at temperatures below $0.8T_c$. However, a significant change in the depth of the dielectric layer was observed, as seen in Fig. 5. For a fluence of 12 J/cm^2 the dielectric layer depth reaches depths of greater than 600 nm.

The absorption of the laser energy in the dielectric layer during nanosecond laser heating was also analyzed for different values of absorption coefficient. The resulting temperature profile is shown in Fig. 6 for several hypothetical values of absorption coefficient. Each of the dielectric layer absorption coefficient values given is stated in terms of the percentage of the room-temperature metallic value. When the absorption coefficient was set to values greater than 1% of the metallic value of a, the surface temperature increased quickly above $0.8T_c$ and reached $0.9T_c$ in less

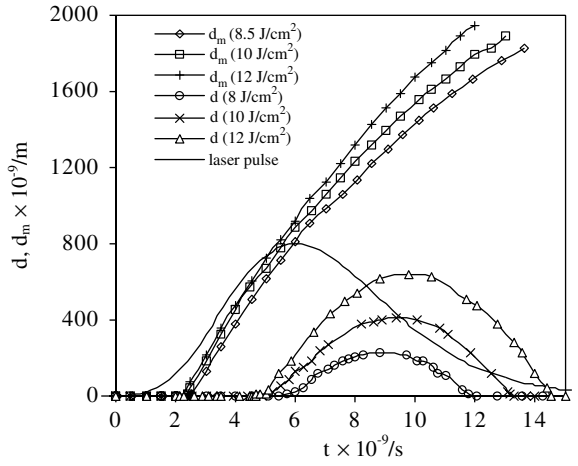

Fig. 5. Melting depth (d_m) and dielectric layer thickness (d) for different incident laser fluences ($a_d = 1676$ m^{-1}, $\tau = 7$ ns (FWHM)).

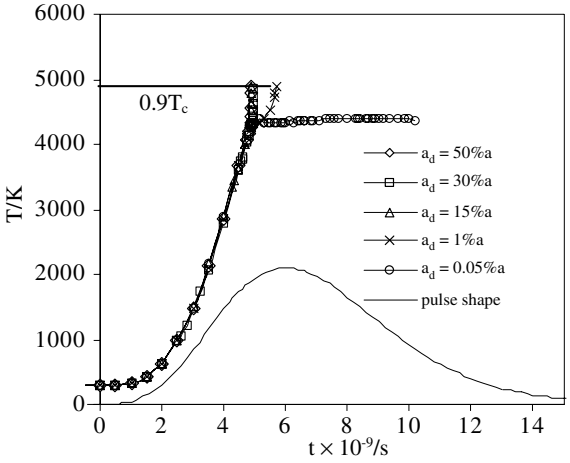

Fig. 6. Transient surface temperature for different values of the absorption coefficient in the dielectric layer ($\tau = 7$ ns (FWHM), laser fluence 10 J/cm^2).

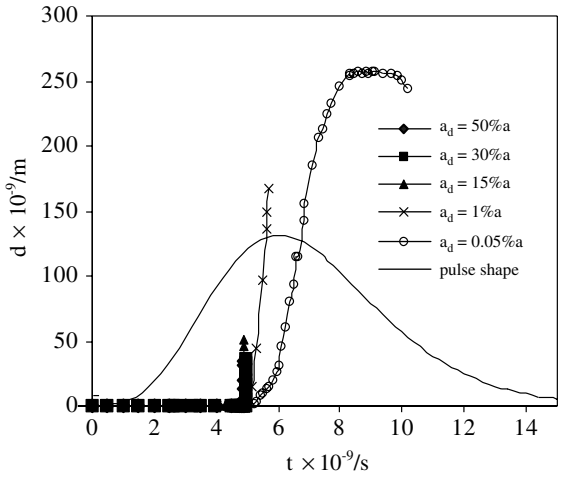

Fig. 7. Transient thickness of the dielectric layer for different values of the absorption coefficient ($\tau = 7$ ns (FWHM), laser fluence 10 J/cm^2).

than 1 ns. However the temperature slightly increased but still remained below $0.9T_c$ when values of absorption coefficient smaller than 0.05% of a were used (which is only slightly higher than that predicted by Eq. (14)). The sharp increase in temperature above $0.8T_c$ can be explained by the increase of the absorbed radiation and the decrease of surface reflectivity at $0.8T_c$. In this work, calculations were stopped for any simulation when the surface temperature reached $0.9T_c$. Once the surface temperature reached this value, the simulations were no longer valid due to the explosive liquid–vapor phase change that results from homogeneous nucleation. Thus, the numerical data for temperature and dielectric layer depth are truncated when the simulation reached $0.9T_c$, as observed in Figs. 6 and 7 (and later in Figs. 11 and 12).

Fig. 7 plots the transient dielectric layer thickness for several values of the absorption coefficient. When the absorption coefficient was set to values greater than 1% of a, the dielectric layer thickness ranged from a maximum of 160 nm to as low as 50 nm for a laser fluence of 10 J/cm^2. The dielectric layer growth was limited by the surface temperature, which reached $0.9T_c$ soon after the dielectric transition was initiated a $0.8T_c$.

5.2. Picosecond heating

Fig. 8(a) shows transient surface temperature induced by a laser pulse of 50 ps (FWHM) without considering dielectric transition at $0.8T_c$. It was found that the laser fluence required to reach phase explosion threshold ($0.9T_c$) is 510 mJ/cm^2. When the dielectric transition was considered in the model, significant changes in surface temperature were found. Assuming that the dielectric layer is transparent to the laser radiation ($a_d = 0$), the surface temperature never increases above $0.8T_c$, as seen in Fig. 8(b), similar to the results for nanosecond heating. However, for a laser fluence of 800 mJ/cm^2, a dielectric layer was formed during the laser pulse and grew to a maximum depth of approximately 35 nm as shown in Fig. 9. When the absorption coefficient of the dielectric layer was set to a value of $a_d = 1675\ \mathrm{m}^{-1}$ as predicted by Eq. (14), the dielectric thickness shown in Fig. 10 was not significantly altered from those seen in Fig. 9. Results similar to those obtained during nanosecond laser heating were obtained for different values of absorption coefficient. Fig. 11 shows that when the absorption coefficient was set to values greater than 1% of the metallic value of$a$, the surface temperature increased quickly above $0.8T_c$ and reached $0.9T_c$ in less than 5 ps. The sharp increase of surface temperature to $0.9T_c$ interrupts the growth of the semitransparent layer soon after the dielectric transition is initiated at $0.8T_c$, as seen in Fig. 12. The maximum dielectric layer thickness that might be obtained during picosecond heating regime is approximately 30 nm for a laser fluence of 700 mJ/cm^2 and considering an

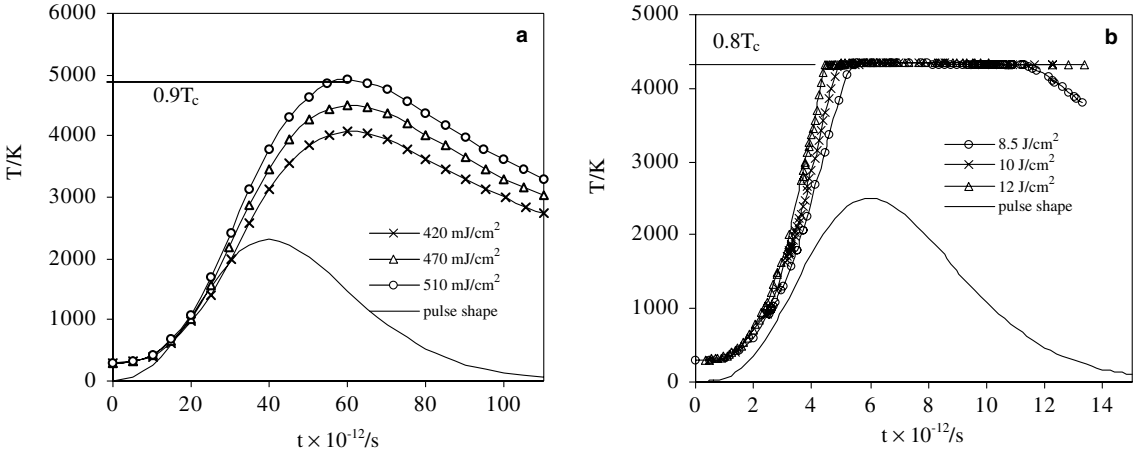

Fig. 8. Transient surface temperature for different laser fluences: (a) without considering dielectric transition; (b) considering dielectric transition at $0.8T_c$ ($\tau = 50$ ps (FWHM)).

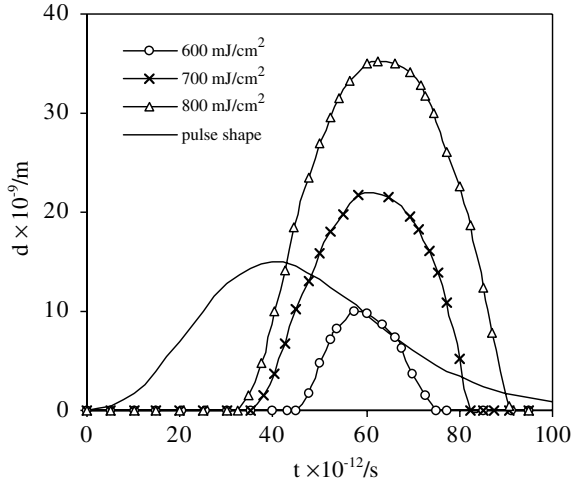

Fig. 9. Transient thickness of the dielectric layer for different incident laser fluences ($a_d = 0$, $\tau = 50$ ps (FWHM)).

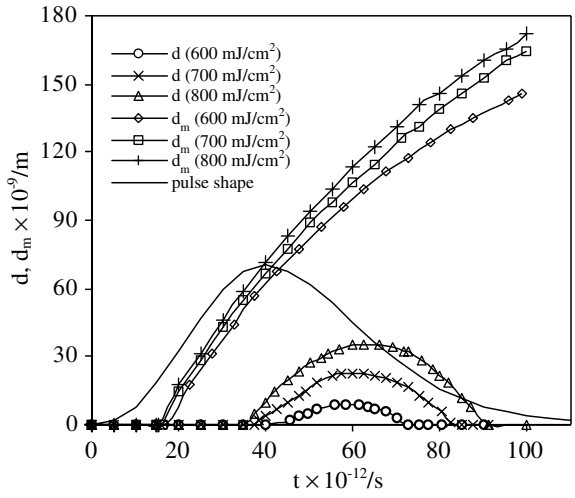

Fig. 10. Melting depth (d_m) and dielectric layer thickness (d) for different incident laser fluences ($a_d = 1676\ m^{-1}$, $\tau = 50$ ps (FWHM)).

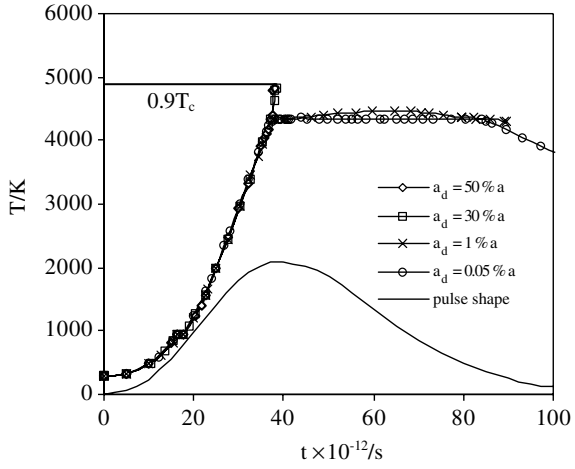

Fig. 11. Transient surface temperature for different values of the absorption coefficient in the dielectric layer ($\tau = 50$ ps (FWHM), laser fluence 700 mJ/cm^2).

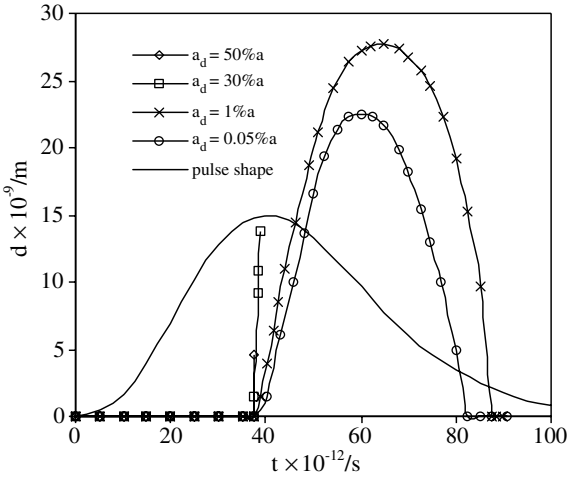

Fig. 12. Transient thickness of the dielectric layer for different values of the absorption coefficient ($\tau = 50$ ps (FWHM), laser fluence 700 mJ/cm^2).

absorption coefficient of about 1% of the metallic value of a.

6. Conclusions

This study demonstrates the importance of dielectric transition when calculating the laser fluence to reach $0.9T_c$ for time scales ranging from nanoseconds to picoseconds. When a zero or a small absorption coefficient, as predicted by Batanov (Eq. (14)), was used for the dielectric layer, the surface temperature did not increase above $0.8T_c$ and a dielectric liquid layer was formed on the surface and was present only during the laser pulse. Any further increase in fluence would only increase the depth of the dielectric layer while the surface temperature will remain constant at approximately $0.8T_c$. Therefore, the model shows that phase explosion is not likely to occur if the dielectric layer is characterized by a near-zero absorption coefficient. Similar results were found for the picosecond laser heating. Since, experimental studies have shown that phase explosion occurs during the laser pulse during ablation of metals [8], it is likely that the absorption coefficients predicted by Batanov et al. [9] under-predict the laser beam absorption and heating in the dielectric layer. However, a dielectric layer absorption coefficient with a value of only 1% of the room temperature value results in significant absorption in the dielectric layer, allowing the surface temperature to reach $0.9T_c$. It was shown that the laser fluence required to reach $0.9T_c$ in both nanosecond and picosecond laser heating regimes is very sensitive to the absorption coefficient chosen to characterize the dielectric liquid. A correct value for the laser fluence required to reach $0.9T_c$ can not be calculated without an exact value for the absorption coefficient of the dielectric layer. Although Batanov's prediction of the dielectric layer absorption coefficient may have been close, more accurate knowledge of optical properties are required for improved prediction of phase explosion threshold.

References

[1] A. Miotello, R. Kelly, Critical assessment of thermal models for laser sputtering at high fluences, Appl. Phys. Lett. 67 (1995) 3535–3537.

[2] M.M. Martynyuk, Liquid–vapor and metal–dielectric transitions in mercury, Russian J. Phys. Chem. 49 (10) (1975) 1545–1547.

[3] W. Fucke, U. Seydel, Improved experimental determination of critical-point data for tungsten, High Temperatures High Pressures 12 (1980) 412–432.

[4] M.M. Martynyuk, Vaporization and boiling of liquid metal in an exploding wire, Sov. Phys. Technical Phys. 19 (1974) 793–797.

[5] D.A. Willis, X. Xu, Heat transfer and phase change during picosecond laser ablation of nickel, Int. J. Heat Mass Transfer 45 (2002) 3911–3918.

[6] X. Xu, G. Chen, K.H. Song, Experimental and numerical investigation of heat transfer and phase change during excimer laser interaction with nickel, Int. J. Heat Mass Transfer 42 (1999) 1371–1382.

[7] N.M. Bugakova, A.V. Bulgakov, Pulsed laser ablation of solids: transition from normal vaporization to phase explosion, Appl. Phys. A 73 (2001) 199–208.

[8] K.H. Song, X. Xu, Explosive phase transformation in excimer laser ablation, Appl. Surf. Sci. 127–129 (1998) 111–116.

[9] V.A. Batanov, F.V. Bunkin, A.M. Prokhorov, V.B. Fedorov, Evaporation of metallic targets caused by intense optical radiation, Sov. Phys. JETP 36 (2) (1973) 311–322.

[10] J.H. Yoo, S.H. Jeong, X.L. Mao, R. Greif, R.E. Russo, Evidence for phase-explosion and generation of large particles during high power nanosecond laser ablation of silicon, Appl. Phys. Lett. 76 (2000) 783–785.

[11] T.Q. Qiu, C.L. Tien, Heat transfer mechanisms during short-pulse laser heating of metals, J. Heat Transfer 115 (1993) 835–841.

[12] E.G. Dwight (Ed.), American Institute of Physics Handbook, third ed., McGraw-Hill, New York, 1972, pp. 4-112–4-113.

[13] B. Rethfeld, A. Kaiser, M. Vicanek, G. Simon, Ultrafast dynamics of nonequilibrium electrons in metals under femtosecond laser irradiation, Phys. Rev. B 65 (2002) 214303-1–214303-11.

[14] M. Von Allmen, A. Blatter, Laser-beam Interactions with Materials Springer Series in Materials Science, second ed., vol. 2, Springer-Verlag, 1995, p. 119.

[15] S.I. Anisimov, Vaporization of metal absorbing laser radiation, Sov. Phys. JETP 36 (1) (1968) 182–183.

[16] M.F. Modest, Radiative Heat Transfer, McGraw-Hill, Inc., New York, 1993, pp. 92–102.

[17] H.Z. Zhuang, X.W. Zou, Z.Z. Jinn, D.C. Tian, Metal–nonmetal transition of fluid Cs along the liquid–vapour coexistence curve, Physica B 253 (1998) 68–72.

[18] A.N. Mostovych, Y. Chan, Reflective probing of the electrical conductivity of hot aluminum in the solid, liquid, and plasma phases, Phys. Rev. Lett. 79 (25) (1997) 5094–5097.

[19] E.A. Brandes, G.B. Brook (Eds.), Smithells Metals Reference Book, Butterworth Heinemann, Oxford, 1992, 14-1–14-3.11.